

How and what to learn — The modes of machine learning

Sihan Feng, Yong Zhang, Fuming Wang and Hong Zhao*

Department of Physics, Xiamen University, Xiamen 361005, Fujian, China

[*zhaoh@xmu.edu.cn](mailto:zhaoh@xmu.edu.cn)

Despite their great success, there is still no comprehensive understanding of machine learning. Here we proposal a new approach, namely the weight pathway analysis (WPA), to study the mechanism of recognition and classification of multilayer neural networks. Instead of neurons or weight edges, we consider weight pathways linking neurons longitudinally from input neurons to output neurons as the basic units of a neural network. We decompose a neural network into a series of subnetworks of weight pathways that have either a hidden-layer neuron or an output-layer neuron as node, and then establish characteristic maps for these subnetworks. The characteristic map characterizes the enhancement or suppression of the influence of each component of an input vector over the hidden-layer neuron or the output-layer neuron, and at the same time reveals the internal coherence structure of the neural network. The parameters of a characteristic map can be visualized, providing a “longitudinal” perspective of the network and making the neural network explainable. Using WPA, we discover that a neural network stores and utilizes information in a "holographic" way, that is, the network encodes all training samples in a coherent structure. An input vector interacts with this "holographic" structure to enhance or suppress each subnetwork which working together to produce the correct activities in the output neurons to recognize the input sample. Furthermore, with WPA, we reveal fundamental learning modes of a neural network: the linear learning mode and the nonlinear learning mode. The former extracts linearly separable features while the latter extracts linearly inseparable features. It is found that hidden-layer neurons self-organize into different classes in the later stages of the learning process. It is further discovered that the key strategy to improve the performance of a neural network is to control the ratio of the two learning modes to match that of the linear and the nonlinear features while avoiding overlearning, and that increasing the width or the depth of a neural network helps this ratio controlling process. This provides theoretical ground for the practice of optimizing a neural network via increasing its width or its depth. WPA gives us a newer and deeper perspective of neural networks, the knowledge gained with WPA enables us to understand the fundamental questions such as what to learn, how to learn, and how can learn well.

INTRODUCTION

In the last decades, learning algorithms have made remarkable progress on numerous machine learning tasks and dramatically improved the state-of-the-art in many practical areas [1]. In addition to practical applications, theoretical studies

striving to understand the mechanism of learning and make the “black-box” of learning models transparent are receiving increased attention [2-4]. Researchers have carried out studies from various angles, including mutual information [5,6], the hidden manifold model [7,8], statistical mechanics [9,10], mean-field theory [11], etc.. These investigations deepened our understanding of the learning mechanism, but we are only beginning to have some understanding of it [2,3]. In particular, although various methods and strategies to improve the performance of learning models have been tried, such as increasing the width and the depth of the network, using the smallest possible learning rate, etc., it is not fully clear why would these methods work or to what extent will they work. To advance in this area, researches on interpretability and explainability of the training process, learned representations, and decisions with human-interpretable explanations have developed into a subfield of machine learning [12,13]. Recently there has been a return to simple models, particularly linear models such as Deep Matrix Factorization [14,15], for gaining the better interpretability. These studies have achieved great success. However, linear models suffer from low predictivity, and more essentially, the success of machine learning is mainly due to the application of nonlinear models. Therefore, to develop explanation methods applicable for both linearly separable and linearly inseparable features and to investigate the difference between the learning of these two kinds of features are important.

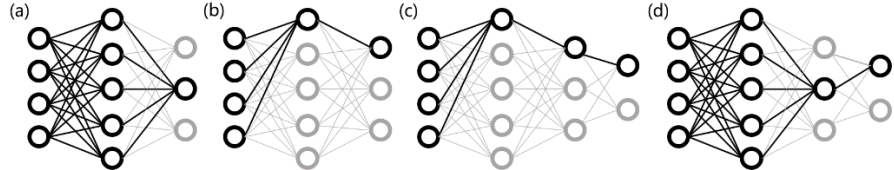


Fig.1 Network of weight pathways, (a) a subnetwork of an output neuron, (b)-(d) subnetworks of a hidden-layer neuron. Networks connections are represented by dark solid lines.

We present a framework based on the concept of weight pathways to study neural networks; we call it weight pathway analysis (WPA). Different from previous layer by layer analyzing approaches [16,17], we establish a “longitudinal” radiographic view of the network. In more details, considering a neural network shown in Fig. 1, we see that there are pathways between input neurons and output neurons that are connected by weighted edges. We call a path connecting an input neuron and an output neuron via these weighted edges a weight pathway and the product of the weights along the path the weight product of the weight pathway. In the case of a monotonic neuron transport function (which is the common case for machine learning; the idea can be extended to more complex neuron transfer functions), the product of a weight pathway has a monotonic relation to the neural network outputs. Weight pathway view point give us ability to investigate direct relations between inputs and outputs of a network. On the contrary, a single weight or a single layer of weights does not provide sufficient information to infer its contribution to the outputs without further calculation. Therefore, weight pathways instead of single weights or single layers of weights should be treated

as the basic units for understanding a neural network.

With hidden-layer or output-layer neurons as nodes, we decompose a neural network into subnetworks of weight pathways, as examples shown by Fig. 1. Then, we integral all of the weight pathways connecting an input neuron and the output neuron (i.e., sum up the weight products of these weight pathways) and define the value as the penetration coefficient from the input neuron to the output neuron. The penetration coefficients of all of the input neurons to the output neuron of a subnetwork are used to construct a characteristic map of the subnetwork, which characterizes the enhancement or suppression effect of the subnetwork on each input vector component's ability of excite the output neuron of the subnetwork.

We visualize the penetration coefficients of a subnetworks and call it the radiograph of the subnetwork. In the case that samples are two-dimensional images, the penetration coefficients and the image pixels have a one-to-one correspondence, by which one can infer the enhancement or suppression effect of the subnetwork to each pixel. The radiograph gives a "longitudinal" penetrating view of the neural network, making the "black-box" less opaque and more interpretable, as any adjustment or operation to the network can be visualized via the radiograph. The visualization here reflects the structure of the network itself, in other words, the structure of the system parameters, which is different from the famous "mask" method [18], which needs backtracking calculations with the input of specific samples. Such penetrating radiographs enable us to gain important insights on the learning process of neural networks. For example, we discover that subnetworks are "holographic", that is, every training sample is encoded in every subnetwork instead of some training samples encode in some subnetwork or neurons. This discovery provides important information on how the information is stored in a neural network and how new objects are identified.

With the help of penetrating radiographs, we show that hidden-layer neurons self-organize into different classes in order to reduce the cost function. More essentially, we reveal that the network uses a learning mode, we call linear learning mode, for extracting linearly separable features, while uses another learning mode, we call nonlinear learning mode, to extract linearly inseparable features. It is found that linearly separable features can be extracted by single neurons, while linearly inseparable features can only be extracted via cooperation of multiple neurons using the nonlinearity characteristics of their transfer function. As a result, neural networks will always try to extract linear features with linear learning mode first; this explains an important previous finding, that is, the earlier learning stage of a deep neural networks is equivalent to a linear classifier [19,20]. Our study also reveals that the nonlinear learning mode is initiated when linear features are insufficient to further minimize the cost function. Therefore, how to maximize the extraction of linearly separable features and linearly inseparable features is the key to optimize the performance of a neural network. We will show that increasing the width or the depth of a neural network helps this optimization process. This finding provides theoretical ground for the practice of optimizing a neural network via increasing its width or its depth.

This paper is arranged as the following. Section 2 introduces our model and algorithm. Section 3 demonstrates the basic principle of WPA using toy samples and a

three-layer neural network. The linear and nonlinear learning modes, as well as the self-organized classification of hidden-layer neurons, are shown in this section. Section 4 applies WPA to the learning of the MINIST set of the handwritten digits, and explains why increasing the width and depth of a neural network can help maximizing the extraction of linearly separable and linearly inseparable features. Section 5 introduce another approach for monitoring activities of training process, i.e., the degree of attention of learning, as an augmentation to the WPA. The final section gives conclusions and discussions.

1 MODEL and METHOD

In this paper we consider a multi-layer neural network given by following equations,

$$\begin{aligned} x_{i_l}^{(l)} &= f(\beta h_{i_l}^{(l)}) \\ h_{i_l}^{(l)} &= \sum_{i_{l-1}=1}^{N_{l-1}} w^{(l)}_{i_l i_{l-1}} x_{i_{l-1}}^{(l-1)} \end{aligned} \quad (1)$$

where $x_{i_l}^{(l)}$ and $h_{i_l}^{(l)}$ are the output and the local field of the i_l th neuron in the l th layer respectively, $w^{(l)}_{i_l i_{l-1}}$ represents the weight that connects the i_{l-1} th neuron in the $(l-1)$ th layer to the i_l th neuron in the l th layer, and $f(x)$ is the neuron transfer function, N_{l-1} is the number of the neurons in the $(l-1)$ th layer. The weights in each layer are bounded in an interval of $(-1,1)$ and are randomly initialized. Note that we do not involve the neuron bias into the model for sake of the simplicity. Extending the analysis to cases involving biases is straightforward.

Assuming that the training set is consist of P samples $\{(x(\mu), y(\mu)), \mu = 1, \dots, P\}$, where $x(\mu)$ is the input vector of the μ th sample with components $x_{i_0}^{(0)}(\mu)$ ($i_0 = 1, \dots, N_0$), $y(\mu)$ defines its expected state in the output layer. Here we set $y_{i_L}(\mu) = 1$ if this sample belongs to the i_L th class (we call this neuron the label neuron of this class), and $y_{i_L}(\mu) = -1$ otherwise. For the sake of simplicity, we always apply the linear neuron transfer function to the output layer neurons, i.e., set $x_{i_L}^{(L)} = h_{i_L}^{(L)}$, while applying $f(h) = h$ and $f(h) = \tanh(h)$ to the hidden-layer neurons in linear neural networks (LNNs) and nonlinear neural networks (NNNs) respectively. We then define the cost function as

$$S(d) = \frac{1}{P N_L} \sum_{\mu=1}^P \sum_{i_L=1}^{N_L} \left(x_{i_L}^{(L)}(\mu) y_{i_L}(\mu) - d \right)^2, \quad (2)$$

where d is a parameter that controls the gap between the output of the label neuron and that of the other neurons in the output layer. This cost function is equivalent to the

Margin commonly used by support vector machines. Minimizing the cost function to zero gives $x_{i_L}^{(L)}(\mu)y_{i_L}(\mu) = d$ for all of the samples (we call this relation the goal of

training), but as long as $x_{i_L}^{(L)}(\mu)$ is the largest on the label neuron the sample is correctly classified (we call this condition the goal of classification).

The WPA approach is applicable to all learning algorithms in principle. However, in order to clearly demonstrate how to control the transition from linear learning mode to nonlinear learning mode, we use a simple gradient-free algorithm, namely the Monte Carlo (MC) algorithm [21,22]. The algorithm is quite simple: select a weight randomly with equal probability, then change it randomly to a new value; accept the change if it reduces the cost-function and discard it otherwise. The operation is repeated until the minimization of the cost function is achieved. Because each update is judged by all samples, the cost-function will be reduced monotonously. Besides, since the changed neurons induced by the mutation involves only those connected by weight paths involving the mutated weight, the computation time is acceptable for neural networks with few hidden layers [21].

Since there is no need of differentiation and back-propagation in this algorithm, we can limit the range of weights, for example, by setting $|w^{(l)}_{i_l i_{l-1}}| \leq 1$. Then, with an appropriate transfer function coefficient β , we can control the input-output sensitivity of the network to avoid the overlearning. Due to the restriction of the norm of the weights, linearly separable feature of a sample cannot be amplified infinitely, and thus the cross-over transition from the linear to nonlinear learning modes can be clearly shown by increasing the parameter d . Furthermore, with the limitation on the input-output sensitivity of the network, the width of the network can be greatly increased without overlearning. On the contrary, traditional algorithms, such as the back-propagation (BP) algorithm, does not have these properties. Therefore, although its training speed is not as fast as other traditional algorithms, the MC algorithm is more suitable for studying the mechanism of the machine learning due to its flexibility.

2 RESULTS

2.1 Weight pathways and visualization of penetration coefficients

We call weight edges $w_{i_1 i_0}^{(1)} \rightarrow w_{i_2 i_1}^{(2)} \rightarrow w_{i_3 i_2}^{(3)} \rightarrow \dots \rightarrow w_{i_L i_{L-1}}^{(L)}$ that connects the i_0 th neuron in the input layer to the i_L th neuron in the output layer a weight pathway. We use the product of the weights $w_{i_1 i_0}^{(1)} w_{i_2 i_1}^{(2)} w_{i_3 i_2}^{(3)} \dots w_{i_L i_{L-1}}^{(L)}$ to characterize a weight

pathway and call it the weight product. We call a weight pathway a positive pathway (p-pathway) if its weight product is positive, otherwise a negative pathway (n-pathway). We divide a neural network into subnetworks. Each subnetwork connects all of the input neurons to an output neuron, as illustrated in Fig. 1.

We then define

$$c_{i_0 i_L}^{(i_l, l)} = \left[\sum_{i_1, i_2, \dots, i_{l-1}} w_{i_1 i_0}^{(1)} w_{i_2 i_1}^{(2)} w_{i_3 i_2}^{(3)} \dots w_{i_l i_{l-1}}^{(l)} \right] w_{i_{l+1} i_l}^{(l+1)} \dots w_{i_L i_{L-1}}^{(L)}$$

as the penetration coefficient of a subnetwork from the i_0 th input neuron to the i_L th output neuron, where the summation is over all of the weight pathways that come out from the i_0 th input neuron, go through the i_l th neuron in the l th layer, and end with the i_L th output neuron. Note that the summation covers all hidden-layer neurons between the i_0 th input neuron and the i_l th neuron in the l th layer. Depending on the selection of l , we can have summation over weight pathways that pass through all the hidden-layer neurons ($l=L$) as in Fig. 1(a), over a single weight pathway from an input to an output ($l=1$) as in Fig. 1(b) and 1(c), or over weight pathways through a portion of the hidden neurons ($1 < l < L$) as in Fig. 1(d).

The most important feature of a weight pathway is that it connects the input and the output of a neural network. In the case of monotonic neuron transport functions, the weight products of the weight pathways monotonously determine the direction of the evolution of the local field of an output neuron that shared by the weight pathways, and thus determines the evolution of the cost function. As a result, when we input the μ th sample, the contribution of its i_0 th component $x_{i_0}^{(0)}(\mu)$ to the local field $h_{i_L}^{(L)}(\mu)$ of the i_L th neuron in the output layer is proportional to $c_{i_0 i_L}^{(i_l, l)} x_{i_0}^{(0)}(\mu)$, and the map,

$$H_{i_L}^{(i_l, l)}(\mu) = \sum_{i_0=1}^{N_0} c_{i_0 i_L}^{(i_l, l)} x_{i_0}^{(0)}(\mu), \quad (4)$$

characterizes the contribution of the whole subnetwork to the local field $h_{i_L}^{(L)}(\mu)$. Note that in the particular case of $l=L$ (as in the case of Fig. 1(a)), for a LNN, $H_{i_L}^{(i_L, L)}(\mu) = h_{i_L}^{(L)}(\mu)$, and for a NNN $H_{i_L}^{(i_L, L)}(\mu) \propto h_{i_L}^{(L)}(\mu)$. Therefore, penetration coefficients characterize the influence of each component of an input vector on an output neuron by a specific subnetwork of weight pathways; it helps us to infer whether such an input component's influence over that output neuron is positive or negative by the subnetwork. By decomposing a neural network into subnetworks, we can investigate how each part of the neural network works individually and cooperatively to achieve the goal of classification and the goal of training.

Suppose samples are given by images (with single grey channel) that consist of $M \times M$ bitmap pixels, and the representation vector of the μ th sample is coded as $(x_{i_0}^{(0)}(\mu), i_0 = M\alpha + \beta, \alpha = 1, \dots, M, \beta = 1, \dots, M)$. By plotting a two-dimensional heat map as the following

$$l_{\alpha\beta}^{(i_l, l)}(i_L) = c_{i_0 i_L}^{(i_l, l)} \quad (5),$$

we have a visualization of the penetration coefficients. Note that penetration coefficient $c_{i_0 i_L}^{(i_l, l)}$ can either be positive or negative, corresponding to p-pathway dominant or n-pathway dominant respectively, and the corresponding heat map $l_{\alpha\beta}^{(i_l, l)}(i_L)$ pixels are positively displayed (in shades of red pseudo colors) or negatively displayed (in shades of blue pseudo colors) respectively. The resulting heat map image will have patterns of positively or negatively displayed regions, corresponding to regions of input pixels that would be connected to the output neuron with positive or negative penetration coefficients. With these patterns, one can infer the enhancement or suppression effect to a given sample image at the pixel level following the characteristic map. The visualization can be considered a view of the internal structure of a subnetwork. We thus call heat map $l_{\alpha\beta}^{(i_l, l)}(i_L)$ the radiograph of the subnetwork pertaining to the i_l th neuron in the l th layer, and call the patterns in the radiograph the mode of the subnetwork or the mode of this neuron.

2.2 WPA approach

We illustrate the basic principles of the WPA approach with three sets of toy samples. The input samples are 100x100 bitmaps, and they all contain an identical circle at different position. The pixels inside the circle (the face zone) are assigned a value of $e = 1, 2, \text{ or } 3$, while the pixels outside of the circle (the ground zone) are always assigned a value of -1. Fig. 2(a) shows the three samples of the first training set, where circles with value $e=1, 2, \text{ and } 3$ are shown in yellow, light brown and dark brown colors, respectively. There is no overlap between the face regions in first training set. Fig. 2(b) shows the second training set. The difference from the first one is that the face regions of these three samples completely overlap with each other. Fig. 2 (c) shows the third set of training samples. The difference from the first set is that the face regions of the three samples are partially overlapped. Each sample can be vectorized as a $N = 100 \times 100 = 10^4$ dimensional vector. We train a $10^4 - 200 - 3$ neural network to perform the task of classification; the cost function is defined by (2). Each sample represents one class; the first to the third output neurons are the label neurons of the first to the third sample or class, respectively. The achievement of classification means $h_{i_2}^{(2)}(\mu)$ is the largest if $\mu = i_2$, while the achievement of the training goal means $h_{i_2}^{(2)}(\mu)y_{i_2}(\mu) = d$. It will be seen that the second sample of the second set is linearly inseparable, and the second sample of the third set has both linearly separable and inseparable features. All the other samples are linearly separable.

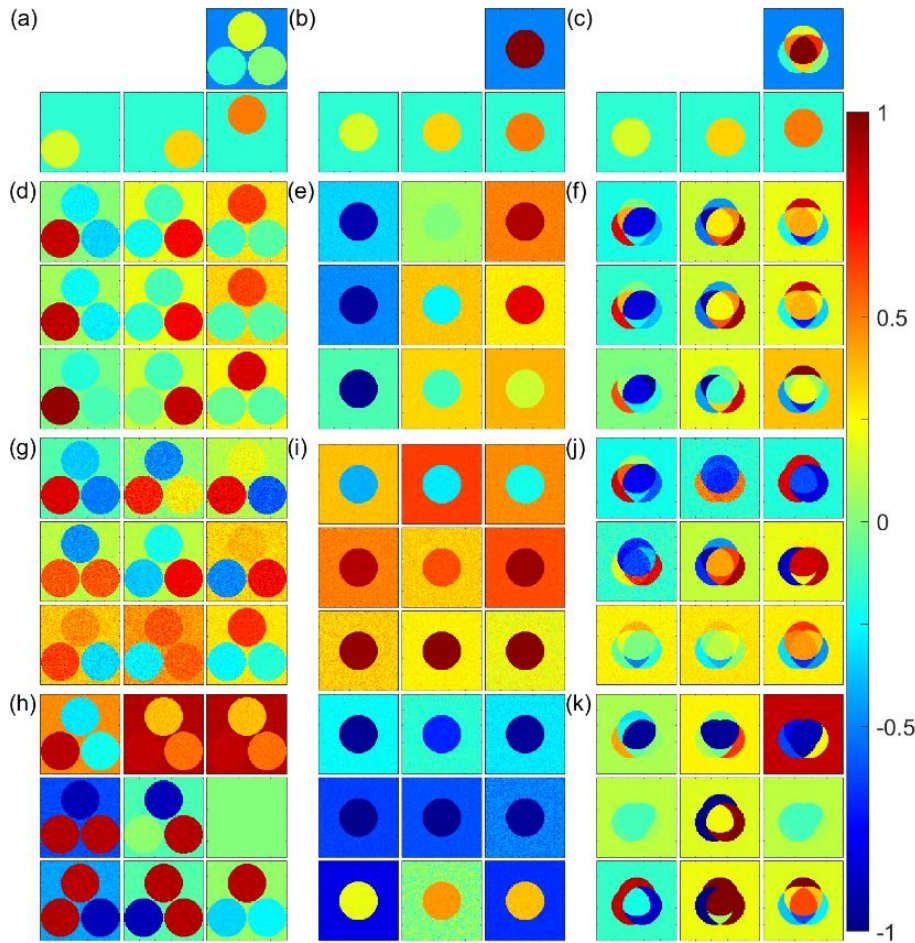


Fig. 2 The visualization of penetrating coefficients. (a)-(c) show the first, second, and third sample sets. The first line gives overlap images of the three samples. (d)-(f) show scenographs of penetrating coefficients of subnetworks for the three sample sets, respectively. The first to the third columns are for the first to the third output neurons. The first to third rows are for the LNN30, the NNN30 and NNN200, respectively. (g) shows scenographs of penetrating coefficients of subnetworks of hidden-layer neurons classified by the LNI for the NNN30. The plots are managed flowing the order of the matrix $\Pi(\mu|i_2)$ with $i_2, \mu = 1, 2, 3$. (h) is same as (g) but for the NNN200. (i) shows the scenographs of penetrating coefficients of subnetworks of hidden-layer neurons of the C_1 to C_6 classes for the second sample set and the NNN30. Here the first to third columns are for the first to third output neurons. (j) and (k) are same as (g) and (h) but for the third sample sets.

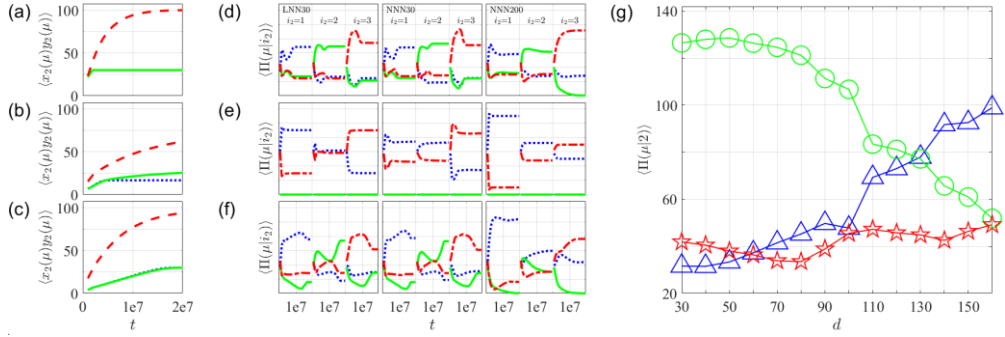


Fig. 3 The transition from the linear learning mode to the nonlinear learning mode. (a)-(c) show $\langle x_{i_L}^{(2)}(\mu) y_{i_L}(\mu) \rangle$ as a function of training time (MC steps) for the three sample sets, respectively. The solid(green), dot lines(blue) and dashed(red) lines for the LNN30, the NNN30 and the NNN200. (d)-(f) show the LNI for the three sample sets, respectively. The first, second and third columns are for the LNN30, the NNN30 and the NNN200, respectively. The parameter i_2 indicates the order of the output neuron. (g) The transition from the phase of the linear learning mode to the mixture phase of linear and nonlinear learning modes. The triangles, circles, and stars represent $\Pi(1|2)$, $\Pi(2|2)$ and $\Pi(3|2)$ obtained after these quantities become stationary after a sufficient long training times.

As a reference, we first train these three training sets with linear neurons of $f(h)=0.002h$ and with $d=30$. We shorthand this neural network as LNN30. In Fig. 3(a)-3(c), we show the evolution of local fields of output neurons $\langle x_{i_L}^{(2)}(\mu) y_{i_L}(\mu) \rangle$ with training time as blue dotted lines. Here, $\langle \cdot \rangle$ is averaged over the three samples and three output neurons. We see that the goal of training is reached for both the first and the third sets. For the second set, it has $\langle x_{i_L}^{(2)}(\mu) y_{i_L}(\mu) \rangle \approx 20$. Averaging only over the three samples, we found that $\langle x_1^{(2)}(\mu) y_1(\mu) \rangle \approx \langle x_3^{(2)}(\mu) y_3(\mu) \rangle \approx 30$ for the first and the third output neurons, but $\langle x_2^{(2)}(\mu) y_2(\mu) \rangle \approx 0$ for the second output neuron. It can be checked that the output of the second sample is never the largest.

We then train these training sets with nonlinear neurons of $f(h)=\tanh(0.002h)$ and with $d=30$. We shorthand this neural network as NNN30. The local fields of output neurons $\langle x_{i_L}^{(2)}(\mu) y_{i_L}(\mu) \rangle$ are shown as green solid lines in Fig. 3(a)-3(c). It can be seen that the goal of training is also completely fulfilled for the first and third training sets. For the second training set, it has $\langle x_{i_L}^{(2)}(\mu) y_{i_L}(\mu) \rangle \approx 28$. Again, averaging only over the three samples we find that $\langle x_1^{(2)}(\mu) y_1(\mu) \rangle \approx \langle x_3^{(2)}(\mu) y_3(\mu) \rangle \approx 30$, and $\langle x_2^{(2)}(\mu) y_2(\mu) \rangle \approx 25$. Thus, both the goal of classification and the goal of training are

fully achieved for the first and the third samples. The goal of training is not fully achieved for the second sample; however, it can be checked that $x_2^{(2)}(2)$ is larger than $x_2^{(2)}(1)$ and $x_2^{(2)}(3)$, i.e., the goal of classification is achieved. When d is increased to $d=200$ (We shorthand this neural network as NNN200), the goal of classification is achieved for all training sets, but the goal of training is not fully achieved by any of the training sets., as shown by the red dashed lines in Fig.3(a)-(c). For the first and third sets, $\langle x_{i_L}^{(2)}(\mu)y_{i_L}(\mu) \rangle \approx 100$. In detail, it can be checked that $\langle x_1^{(2)}(\mu)y_1(\mu) \rangle \approx \langle x_2^{(2)}(\mu)y_2(\mu) \rangle \approx \langle x_3^{(2)}(\mu)y_3(\mu) \rangle \approx 100$ for these sets. For the second set, $\langle x_{i_L}^{(2)}(\mu)y_{i_L}(\mu) \rangle \approx 70$ and it can be checked that $\langle x_1^{(2)}(\mu)y_1(\mu) \rangle \approx 90$, $\langle x_2^{(2)}(\mu)y_2(\mu) \rangle \approx 50$ and $\langle x_3^{(2)}(\mu)y_3(\mu) \rangle \approx 75$, where $\langle \cdot \rangle$ is averaged over the three samples.

2.2.1 Holographic structure

After all the training have finished, we show radiographs of subnetworks of the three output neurons $l_{\alpha\beta}^{(1,2)}(1)$, $l_{\alpha\beta}^{(2,2)}(2)$, and $l_{\alpha\beta}^{(3,2)}(3)$ for the LNN30, the NNN30, and the NNN200 in Fig.2 (d)-2(f), where the columns correspond to the output neurons and the rows correspond to the three types of neural network. For better visualization, we calculate an ensemble average of penetration coefficients of 16 replicas of neural networks for each training set. We see that each visualization image clearly shows the patterns of all the samples in the training set, indicating that each subnetwork "holographically" encodes all samples of a training set. Some zones are positively displayed while others are negatively displayed, implying that the subnetwork of weight pathways establishes coherent structures for enhancement or suppression of different features. The "holographic" structure reveals how a neural network stores information, and indicates that classifications are achieved through the interaction between the input samples and the "holographic" structure. In the following, we will explain how the "holographic" structures are formed and in what a way they work.

2.2.2 The extraction of linearly separable feature and the classification of hidden-layer neurons.

We study the first training set in this section. For this set, the characteristic map can be decomposed into four parts, $H_{i_2}^{(i_L,l)}(\mu) = c(G)x(G) + c(F_1)x(F_1) + c(F_2)x(F_2) + c(F_3)x(F_3)$, which respectively represent the contributions of the

common ground zone (zone G), the face zone of the first sample (zone F_1), the face zone of the second sample (zone F_2), and the face zone of the third sample (zone F_3). Here $c(G)$, $c(F_1)$, $c(F_2)$ and $c(F_3)$ is obtained by summarizing the penetration coefficients within the zone, i.e., $\sum_{i_0} c_{i_0 i_L}^{(i_L)}$, over the zones of G, F_1 , F_2 and F_3 zones, respectively. From Fig 2(d) we see that the polarity of each zone stays the same for all three rows, meaning that the modes of output neurons of either the LNN or the NNNs with a small d and a large d are almost same.

How the goal of classification is achieved can be revealed by the patterns of the radiographs shown in Fig. 2(d). These patterns indicate the modes of the three output neurons. As the positive and negative penetration coefficients represent the enhancement or the suppression effect, the signs of $c(G)$, $c(F_1)$, $c(F_2)$ and $c(F_3)$ thus are essential and are employed to represent the mode of a neuron. From Fig. 2(d) we see that $(\text{sign}(c(G)), \text{sign}(c(F_1)), \text{sign}(c(F_2)), \text{sign}(c(F_3))) = (-, +, -, -)$ $(+, -, +, -)$, and $(+, -, -, +)$ for the three output neurons, respectively. Combining the input values in the four zones $(x(G), x(F_1), x(F_2), x(F_3))$ as $(-1, 1, -1, -1)$, $(-1, -1, 2, -1)$, and $(-1, -1, -1, 3)$ for the first, the second, and the third samples respectively, we know either positive or negative contributions to each output neuron from each zone of an input sample, i.e., we know the signs of the contribution of each zone to $H_{i_2}^{(i,2)}(\mu)$. For example, since the first output neuron has the mode $(-, +, -, -)$, the signs of the contribution from each zone to the characteristic map are $H_1^{(1,2)}(1) \sim (+, +, +, +)$, $H_1^{(1,2)}(2) \sim (+, -, -, +)$, and $H_1^{(1,2)}(3) \sim (+, -, +, -)$, for the first, the second, and the third samples. We see that the contribution from the F_1 zone to $H_1^{(1,2)}(1)$ is positive, while that to $H_1^{(1,2)}(2)$ and $H_1^{(1,2)}(3)$ are both negative.

So as long as $c(F_1)$ is large enough, the condition of $H_1^{(1,2)}(1) > 0$, $H_1^{(1,2)}(2) < 0$ and $H_1^{(1,2)}(3) < 0$ can always be reached. Similar argument can be applied to the second and third output neurons, and one can thus get positive local field for label neurons ($\mu = i_L$) while keeping all the non-label neurons ($\mu \neq i_L$) negative. Hence the goal of classification can always be achieved.

Following the modes of the output neurons, one can construct a linear classification hyperplane for each sample. For example, a vector in the input vector space can be selected as the classification vector, whose components that lie within the G, F_1 , F_2 and F_3 zones have signs of $(-, +, -, -)$, as the signs of $(c(G), c(F_1), c(F_2), c(F_3))$ have. Then, the projection of the first sample to this vector must be the largest among the three input samples. The existence of such classification vectors indicates that samples in this set are all linearly separable. This conclusion is also confirmed by the fact that samples in this training set can be classified by the LNN.

However, the goal of training, i.e., the requirement that $h_{i_2}^{(2)}(\mu)y_{i_2}(\mu) = d$ for each sample as well as for each output neuron, generates additional tasks to the hidden-layer neurons; they will accomplish this goal by working cooperatively. Specifically, the hidden-layer neurons self-organize into classes that are specific to each sample and to each output neuron. One way to capture such self-organization is to count the number of hidden-layer neurons that give the largest contribution to each output neuron when a specific sample is fed to the neural network and study the distribution of such counts. We denote the number of the largest-contribution hidden-layer neurons from input sample μ for the i_2 th output neuron as $\Pi(\mu|i_2)$, and call it largest contribution hidden-layer neuron classification index, or simply the largest neuron index (LNI). Without hidden-layer neuron self-organization, LNI of the label neuron would equal to the total number of hidden-layer neurons while that of the other output neurons would equal to zero. Deviation from such a behavior is an indication of the occurrence of classification of the hidden-layer neurons.

Fig. 3(d) shows the training time evolution of the LNIs of the first, the second, and the third output neurons in the LNN30 for the first training set. In each sub-plot, the solid, dashed and dot lines represents the number of the largest contribution neurons of the first, second and third samples. Similar LNI training time evolutions of the NNN30 and NNN200 are also shown in Fig.3(d). We see that although the label neuron has biggest LNI, i.e., $\Pi(\mu|i_2)$ has the biggest value when $\mu = i_2$, there are still a lot of neurons give their largest contribution to non-label output neurons. This fact reveals the differentiation and self-organization of the hidden-layer neurons.

The classification of hidden-layer neurons can provide more information on how the cost function is minimized. In Fig. 2(g)-2(h), we show radiographs of subnetworks of hidden-layer neurons classified by $\Pi(\mu|i_2)$ for the NNN30 (Fig. 2(g)) and the NNN200 (Fig.2(h)). We denote the radiographs obtained in this way as $l_{\alpha\beta}^{(\Pi(\mu|i_2),1)}(\mu)$, where $\Pi(\mu|i_2)$ specifies the class of hidden-layer neurons. The radiographs for the LNN are similar to that of NN30 and are not shown here. Taking the first output neuron of the NNN30 as an example (the first column of Fig.2(g)), we see that the radiograph $l_{\alpha\beta}^{(\Pi(1|1),1)}(1)$ (the first row and the first column of Fig.2(g)) shows mode of $(c(G), c(F_1), c(F_2), c(F_3)) \sim (-, +, -, -)$, which is the same as that of $l_{\alpha\beta}^{(1,2)}(1)$. With this mode the characteristic map gives $H_1^{(\Pi(1|1),1)}(1) \sim (+, +, +, +)$, $H_1^{(\Pi(1|1),1)}(2) \sim (+, -, -, +)$, and $H_1^{(\Pi(1|1),1)}(3) \sim (+, -, +, -)$ for the first, the second, and the third samples. Since this class of neurons has the largest population (Fig. 3(d)), it can achieve the goal of classification, as discussed early. We call these hidden-layer neurons the dominant neurons. Meanwhile, the radiograph $l_{\alpha\beta}^{(\Pi(2|1),1)}(1)$ (the second row and the first column of Fig.2(g)) shows the mode of

$(c(G), c(F_1), c(F_2), c(F_3)) \sim (+, +, +, -)$. The characteristic map gives $H_1^{(\Pi(2|1),1)}(1) \sim (-, +, -, +)$, $H_1^{(\Pi(2|1),1)}(2) \sim (-, -, +, +)$, and $H_1^{(\Pi(2|1),1)}(3) \sim (-, -, -, -)$. The radiograph $l_{\alpha\beta}^{(\Pi(3|1),1)}(1)$ (the third row and the first column of Fig.2(g)) shows the mode of $(c(G), c(F_1), c(F_2), c(F_3)) \sim (+, +, -, +)$. The characteristic map gives $H_1^{(\Pi(3|1),1)}(1) \sim (-, +, -, +)$, $H_1^{(\Pi(3|1),1)}(2) \sim (-, -, +, +)$, and $H_1^{(\Pi(3|1),1)}(3) \sim (-, -, -, -)$. Obviously, the differentiation of hidden-layer neurons provides more freedom to adjust the outputs. For example, neurons of $\Pi(2|1)$ class decreases the output of the third sample, and neurons of $\Pi(3|1)$ class decreases the output of the second sample, leading $h_1^{(2)}(2)$ and $h_1^{(2)}(3)$ move towards $h_1^{(2)}(2) = h_1^{(2)}(3) = -d$. Therefore, hidden-layer neurons with different modes provide more freedom to adjust the outputs to fulfill the goal of training. We call these classes the auxiliary neurons.

For the NNN200, we see the same radiographs of $l_{\alpha\beta}^{(1,2)}(1)$, $l_{\alpha\beta}^{(1,2)}(2)$ and $l_{\alpha\beta}^{(1,2)}(3)$ (see the third row of Fig.2(d)) as those for the NNN30; the time evolutions of LNIs are also similar (see Fig.3(d)), but the radiographs of subnetworks of neurons classified by the LNI show certain significant differences. The G zones of radiographs almost all reverse their sign relative to those of the NNN30. This phenomenon is a result of self-organization for the purpose of maximum minimization of the cost function. From the patterns one can also find out how the self-organization is performed. For example, $\Pi(2|3)$ class almost disappears, so the G zone of $\Pi(1|3)$ class has to become highly positive in order to decrease the local field of the third output neuron when inputting the first and the second samples. Note that due to the limits put on the norm of the weights, the cost function has not been fully minimized to zero.

2.2.3 The extraction of linearly inseparable feature

For the second training set, each sample has only a ground zone (G) and a face zone (F), and we thus can perform a detail analysis about the modes of the neurons before report the results. In this case, a neuron has four possible modes, $(c(G), c(F)) \sim (+, -), (-, +), (+, +), (-, -)$. Since $x(G) = -1$ and $x(F) = 1, 2, 3$ for the three samples, characteristic map $H_{i_2}^{(i_1,l)}(\mu) = c(G)x(G) + c(F)x(F)$ can be determined directly by neuron modes. For example, mode $(+, -)$ leads to

$H_{i_2}^{(i,l)}(\mu) < 0$ and mode $(-, +)$ leads to $H_{i_2}^{(i,l)}(\mu) > 0$ for all three samples. While mode $(+, +)$ has $c(G)x(G) < 0$ and $c(F)x(F) > 0$, and thus $H_{i_2}^{(i,l)}(\mu)$ may have different signs for different samples depending on the amplitudes of $c(G)$ and $c(F)$. In more details, for a fixed value of $c(G)x(G) < 0$, depending on the amplitude of $c(F)$, it has four possible combinations of $H_{i_2}^{(i,l)}(\mu)$ when inputting the three samples, i.e., $H_{i_2}^{(i,l)}(1) < H_{i_2}^{(i,l)}(2) < H_{i_2}^{(i,l)}(3) < 0$; $H_{i_2}^{(i,l)}(1) < H_{i_2}^{(i,l)}(2) < 0$ and $H_{i_2}^{(i,l)}(3) > 0$; $H_{i_2}^{(i,l)}(1) < 0$ and $0 < H_{i_2}^{(i,l)}(2) < H_{i_2}^{(i,l)}(3)$; $0 < H_{i_2}^{(i,l)}(1) < H_{i_2}^{(i,l)}(2) < H_{i_2}^{(i,l)}(3)$. We denote them as $(+, +)_1$, $(+, +)_2$, $(+, +)_3$, and $(+, +)_4$, respectively. Similarly, for the mode $(-, -)$ it has $c(G)x(G) > 0$ and $c(F)x(F) < 0$, and therefore $H_{i_2}^{(i,l)}(\mu)$ may have combinations $0 < H_{i_2}^{(i,l)}(1) < H_{i_2}^{(i,l)}(2) < H_{i_2}^{(i,l)}(3)$; $0 < H_{i_2}^{(i,l)}(1) < H_{i_2}^{(i,l)}(2)$ and $H_{i_2}^{(i,l)}(3) < 0$; $0 < H_{i_2}^{(i,l)}(1)$ and $H_{i_2}^{(i,l)}(2) < H_{i_2}^{(i,l)}(3) < 0$; $H_{i_2}^{(i,l)}(1) < H_{i_2}^{(i,l)}(2) < H_{i_2}^{(i,l)}(3) < 0$. We denote them as $(-, -)_1$, $(-, -)_2$, $(-, -)_3$, and $(-, -)_4$, respectively. Therefore, there are a total of 10 neuron modes for the second training set and that these results are applicable for both linear and nonlinear neurons if the neuron transport function is monotonous.

Therefore, neurons or subnetworks with mode $(-, -)_3$ can achieve the goal of classification for the first sample because $0 < H_{i_2}^{(i,l)}(1)$ and $H_{i_2}^{(i,l)}(2) < H_{i_2}^{(i,l)}(3) < 0$, and neurons or subnetworks with mode $(+, +)_2$ can achieve the goal of classification for the third sample because $H_{i_2}^{(i,l)}(1) < H_{i_2}^{(i,l)}(2) < 0$ and $H_{i_2}^{(i,l)}(3) > 0$. Indeed, these two samples are linearly separable. For example, one can construct a classification vector, whose components that lie within the G and F zones would have signs as $\text{sign}(x(G), x(F)) = \text{sign}(c(G), c(F)) = (-, -)$, then the projection of the first sample to this vector must be the largest among the three input samples because it has the smallest $x(F)=1$.

However, we see that there is no mode that can convert the output of the second sample to the largest value. This is because its face zone is identical to those of the other samples and its pixel value is between that of the first and third ones; therefore, the monotonic transformation cannot make its output largest in any way. In other words, a single neuron or a single subnetwork alone cannot realize the classification of the second sample. This sample is thus linearly inseparable, which is confirmed by the fact that a LNN cannot classify this sample.

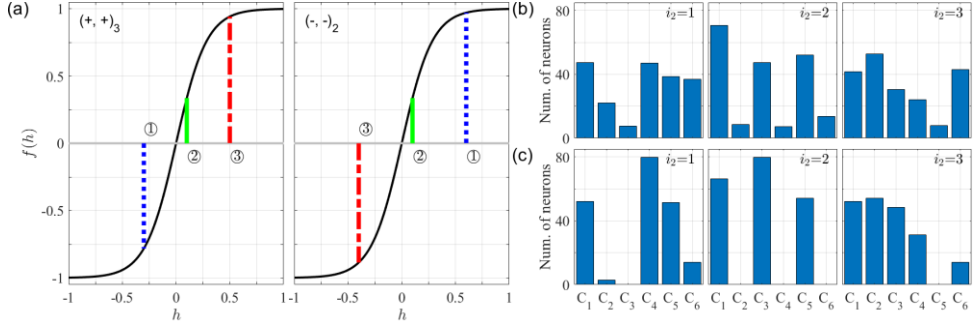


Fig.4 The formation of the nonlinear learning mode. The right-hand and left-hand plots of (a) show the modes of $(+, +)_3$ and $(-, -)_2$ of hidden-layer neurons. (b) and (c) show the number of neurons in the six classes (see text), for the NNN30 and the NNN200, respectively.

Therefore, the fact that the NNN can achieve the goal of classification implies that it makes use of combinations of neurons with different modes. As shown in Fig. 4(a), a pair of neurons with $(+, +)_3$ and $(-, -)_2$ modes can convert the output of the second sample to be the largest, as long as the outputs of the first and third samples lie on the nonlinear region of $\tanh(h) \approx \pm 1$. In this case, the outputs of the first and third samples cancel approximately, while that of the second sample appears as a large positive quantity since both neurons contribute a positive term. It is easy to check that the conversion can also be realized by combinations of $(+, +)_3$ and $(-, -)_3$, $(+, +)_2$ and $(-, -)_2$, though they are less efficient at converting. We emphasize that the nonlinearity of the transfer function plays a key role here. With a linear neural transfer function, $f(h) = kh$, $(+, +)_3$ and $(-, -)_2$ must lead to the combined outputs of the second sample vanishing if one wants to offset the outputs of the first and the third samples.

It is obvious that, for the first output neuron, for example, the goal of training cannot be achieved by neurons only with modes of $(-, -)_3$, since it gives $0 > h_2^{(2)}(2) > h_2^{(2)}(3)$ and thus fails to approach the condition of $h_2^{(2)}(2) = h_2^{(2)}(3) = -d$. Therefore, auxiliary neurons with different mode must be utilized. In Fig.3(e) we show the LNI for this training set. It clearly confirms the differentiation of hidden-layer neurons, as the non-vanishing $\Pi(1|i_2)$ and $\Pi(3|i_2)$ indicate that each output neuron has hidden-layer neurons in different modes. The fact that $\Pi(2|i_2)$ vanishes indicates that there is no single neuron can convert the output of the second sample to be the largest. Note that neurons in a class of $\Pi(\mu|i_2)$ may have several neuron modes. For example, neurons of $\Pi(1|1)$ may involve modes of $(-, -)_2$, $(-, -)_3$ and $(+, +)_4$, since all of them have the largest contribution to the first output neuron from the first input sample. For a more detailed investigation, we can check the distribution of neurons for all of the possible modes. Note that neuron modes of this training set can be divided into six classes: $(+, -)$, $(+, +)_1$ and $(-, -)_4$ leading to negative outputs for all samples and are classified into one class (designated as C_1 class); $(-, +)$,

$(+, +)_4$ and $(-, -)_1$ leading to positive outputs for all samples and are classified into another class (designated as C_2 class); For the rest modes: $(+, +)_2$, $(+, +)_3$, $(-, -)_2$, and $(-, -)_3$, each represents a different class (designated as C_3 , C_4 , C_5 , and C_6 classes respectively). For the sake of simplicity, we calculate the number of hidden-layer neurons of the six classes instead of the 10 modes for the NNN30 and NNN200, and show them in Fig. 4(b)-4(c). This approach provides another classification standard for checking the differentiation. The results reveal more details of the classification of hidden-layer neurons than LNI does.

With these details, we can understand how the classification of hidden-layer neurons is essential for minimizing the cost function. Using the first output neuron as an example again, it can be seen that although $(-, -)_3$ accounts for a large proportion, neurons of all the six classes exist. Neurons with mode $(+, +)_2$ raises the output of the third sample, leading the local fields evolve towards $h_2^{(2)}(2) = h_2^{(2)}(3) = -d$.

The C_1 class decreases the outputs globally, but can also adjust the amplitude of contributions for different samples. In such a way, the local fields evolve towards the goal of minimizing the cost function to zero. For this purpose, neurons with mode $(-, -)_3$ and $(+, +)_2$, as well as the modes in the C_1 class are more essential; therefore, in the case of NNN200, these modes remain but others are suppressed dramatically. Due to the insufficient number of hidden-layer neurons, minimization of the cost function can only give $\langle x_{i_L}(\mu) y_{i_L}(\mu) \rangle \approx 70$, and due to the insufficient number of auxiliary neurons, it has $\langle x_1(\mu) y_1(\mu) \rangle \approx 90$, $\langle x_2(\mu) y_2(\mu) \rangle \approx 50$ and $\langle x_3(\mu) y_3(\mu) \rangle \approx 75$.

In Fig 2 (i), we show radiographs $l_{\alpha\beta}^{(C_i, 1)}(i_L)$ of subnetworks of the 6 classes for the NNN30 as examples. We see that they are in well agreement with the patterns of modes of that class. Note that radiograph $l_{\alpha\beta}^{(i, 2)}(i_L)$ of Fig. 2(e) is the result of superposition of radiographs of the 6 classes. For the first and the third output neurons, since hidden-layer neurons with modes $(-, -)_3$ and $(+, +)_2$ have the largest populations respectively, $l_{\alpha\beta}^{(1, 2)}(1)$ and $l_{\alpha\beta}^{(3, 2)}(3)$ thus show patterns of $(c(G), c(F)) \sim (-, -)$ and $\sim (+, +)$. For the second output neuron, neurons with modes of $(+, +)_3$ and $(-, -)_2$ have roughly equal numbers, (see Fig. 4(b)), patterns resulted by them thus are almost canceled with each other. The pattern of $l_{\alpha\beta}^{(2, 2)}(2)$, $(c(G), c(F)) = (+, -)$, should be caused by neurons of mode $(+, -)$ in the C_1 class. Note that according to Fig. 4(b) this class has a large number of hidden-layer neurons.

Therefore, extracting the linearly separable and inseparable features has an essential difference. For the linearly separable feature, neurons can independently achieve the goal of classification. The differentiation of hidden-layer neurons is for the

purpose of achieving the goal of training. Specifically, for the first training set, a LNN can achieve the goal of classification with similar modes or radiographs as those of a NNN, see Fig.2(d) and Fig3(d). We call this way of learning the linear learning mode. For linearly inseparable features, for example, the second sample of the second training set, the neural network must use a combination of neurons with different mode and relay on the nonlinearity of the neuron transfer function to convert the output to be the largest. Linear networks cannot achieve such a goal. We call this way of learning the nonlinear learning mode. In principle, the nonlinear learning mode can extract both linearly separable and inseparable features; however, the nonlinear learning mode requires more network resources and hence is reserved for the extraction of the nonlinear features or for the purpose of reaching the difficult goal of training. As shown in Fig. 3(b), even in the case of $d = 30$, the goal of $h_2^{(2)}(2) = d$ has not been strictly reached because the number of auxiliary neurons is not sufficient (Fig. 4(c)).

3.2.4 The extraction of co-existing linearly separable and inseparable features.

In the third sample set, the second sample has both linearly separable features (the part of the face zone that do not overlap with any of the face zones of the other samples, which shall be called the unit linear features of the sample, and the part of the face zone that only overlap with some but not all of the face zones of the other samples.) and linearly inseparable features (the part of the face zone that overlap with all of the face zones of the other samples). Therefore, it can be used to investigate how the neural network works in the coexistence of linearly separable and inseparable features. The first and third samples have only linearly separable features. For the convenience of discussion below, we denote zones of the unit linear feature of the three samples by F_1^0 , F_2^0 , and F_3^0 , respectively.

Fig. 3 (f) shows the training time evolution of the LNI in the LNN30, the NNN30, and the NNN200 in the first to the third column, respectively. We see that the LNI of the NNN30 behaves almost exactly as that of the LNN30. Furthermore, Fig. 2 (f) shows that the radiographs of these two neural networks are also qualitatively similar. Therefore, the NNN30 behaves almost identically to that of the LNN30, indicating that the nonlinear network invokes only the linear learning mode and extracts only the linearly separable features.

Radiographs of output neurons can reveal how the linear learning mode works. For example, from $l_{\alpha\beta}^{(2,2)}(2)$ in Fig. 2(f) we see that $C(F_2^0)$ is positive, and $C(F_1^0)$ and $C(F_3^0)$ are negative. Following the characteristic map, the signs of contributions of these zones to the outputs should be $H_2^{(2,2)}(1) \propto x(F_1^0)C(F_1^0) + x(G)C(F_2^0) + x(G)C(F_3^0) \sim (-, -, +)$, $H_2^{(2,2)}(2) \propto x(G)C(F_1^0) + x(F_2^0)C(F_2^0) + x(G)C(F_3^0) \sim (+, +, +)$, and $H_2^{(2,2)}(3) \propto x(G)C(F_1^0) + x(G)C(F_2^0) + x(F_3^0)C(F_3^0) \sim (+, -, -)$,

respectively. Similar to the case of the first sample set, these modes provide the freedom to fulfill the goal of classification, by amplifying only the amplitude of p-pathways in F_2^0 zone for example.

The subnetworks of hidden-layer neurons classified by the LNI reveal more details. In second column of Fig.2(j) we show the radiographs of the three class, $\Pi(1|2)$, $\Pi(2|2)$ and $\Pi(3|2)$, of hidden-layer neurons for NNN30 respect to the second output neuron, respectively. The non-vanishing of $\Pi(1|2)$ and $\Pi(3|2)$ reveal the phenomenon of differentiation. The $\Pi(2|2)$ class takes the dominant population of hidden-layer neurons (see Fig.3(f)), which confirms that the classification information extracted by single neurons and thus should be linearly separable feature. As a result, the $l_{\alpha\beta}^{(2,2)}(2)$ is qualitatively identical to $l_{\alpha\beta}^{(\Pi(2|2),1)}(2)$ since the former is also dominated by the class of $\Pi(2|2)$. The role of classes $\Pi(1|2)$ and $\Pi(3|2)$ is to assist the $\Pi(2|2)$ class to fulfil the goal of training. For example, the center zones of $l_{\alpha\beta}^{(\Pi(2|2),1)}(2)$ and $l_{\alpha\beta}^{(\Pi(3|2),1)}(2)$ are positive, which give positive contributions to the second output from all the samples, of which that of the third sample is the largest since the pixel value of its face zone is the largest. To offset this positive contribution from the third sample, i.e., $h_2^{(2)}(3)$, the face zone of the third sample in $l_{\alpha\beta}^{(\Pi(1|2),1)}(2)$ is negative, and thus the $\Pi(1|2)$ class can decrease the output of the third sample, which provide the freedom to help $h_2^{(2)}(3)$ move towards $h_2^{(2)}(3) = -d$.

These facts indicate that applying a NNN does not necessarily mean the extraction of the linearly inseparable features when both linearly separable and linearly inseparable features exist in the samples. The reason is that the linear learning mode is performed by hidden-layer neurons independently, while the nonlinear learning mode needs to have multiple neurons working cooperatively and thus is more difficult to be manifested. So, if the goal of training can be achieved using only the linear separable features, the neural network would avoid to activate the nonlinear learning mode. Therefore, one may be at risk of losing the information of linear inseparable feature in the case of coexistence of linearly separable and inseparable features even using a NNN.

However, since we limit the norm of weights, and thus limit the products of weight pathways. Once the parameter d exceeds a threshold, weight pathways connecting only the linearly separable zones will not be able to fulfil the goal of training. In this case, the neural network has to initiate the nonlinear learning mode to extract the linearly inseparable features to further drive the local fields towards the goal of training. For the NNN200, we see from Fig.2(f) and Fig. 3(f) that there is no substantial change for the first and the third output neurons for both the radiographs and the LNI's, indicating that the neural network still extracts information with the linear learning mode, since in these cases all the information are the linearly separable feature. However, remarkable changes can be seen in the case of second output neuron. The center zone of $l_{\alpha\beta}^{(2,2)}(2)$ changes to the same pseudo-color as that of the second sample set ($l_{\alpha\beta}^{(2,2)}(2)$ for the two

NNNs, see Fig. 2(e)). Fig. 3(f) shows that the $\Pi(2|2)$ is no longer the largest, instead, $\Pi(1|2)$ turns to be the largest as in the case of the second sample set (see Fig. 3(e) for the two NNNs).

These facts indicate that the nonlinear learning mode is initiated for the second sample, i.e., the features of the center zone of this sample begins to contribute to the local field $h_2^{(2)}(2)$, which can be observed more clearly by studying radiographs of subnetworks of hidden-layer neurons classified by the LNI. Fig. 2 (k) shows these images for the NNN200. It is seen that $l_{\alpha\beta}^{(2,2)}(2)$ and $l_{\alpha\beta}^{(\Pi(1|2),1)}(2)$ have the same patterns, as a result of $\Pi(1|2)$ class being the dominant population of neurons. The radiograph of $\Pi(2|2)$ shows non-substantial changes to that of the NNN30, indicating that the main role of this class is still for extracting the linearly separable features of the second sample. But radiographs of $\Pi(1|2)$ and $\Pi(3|2)$, i.e., $l_{\alpha\beta}^{(\Pi(1|2),1)}(2)$ and $l_{\alpha\beta}^{(\Pi(3|2),1)}(2)$, have changed substantially from that of Fig. 2(j), indicating a different learning mode is involved. For the $\Pi(1|2)$ class, by definition, each neuron gives the largest contribution to the second output neuron with the input of the first sample. The center zone of its radiograph $l_{\alpha\beta}^{(\Pi(1|2),1)}(2)$ is negative, making contribution from the third sample to the same output neuron the most negative or the smallest in value. In addition, from the radiograph we see that the unit linear feature zone F_2^0 is positive, and thus making the contribution from the second sample larger. As a result, for this class we have $H_2^{(\Pi(1|2),1)}(1) > H_2^{(\Pi(1|2),1)}(2) > H_2^{(\Pi(1|2),1)}(3)$. Similar analysis can lead to $H_2^{(\Pi(3|2),1)}(1) < H_2^{(\Pi(3|2),1)}(2) < H_2^{(\Pi(3|2),1)}(3)$ for the $\Pi(3|2)$ class. Therefore, these two classes of neurons play the role of modes $(+, +)_3$ $(-, -)_2$ in Fig. 4 and perform the extraction of the linearly inseparable features of the second sample in this sample set.

Therefore, in the case of the NNN30, the majority of the hidden-layer neurons is employed to extracting the linearly separable feature. The goal of training is achieved by this kind of neurons with the help of some auxiliary neurons, and the excitation of the nonlinear learning mode is not necessary. In the case of the NNN200, the goal of training cannot be achieved by learning just the linearly separable features, and the nonlinear learning mode has to be initiated. In Fig 3(g), we plot $\Pi(1|2)$, $\Pi(2|2)$ and $\Pi(3|2)$ of the NNN as a function of control parameter d . Each data point is obtained after the training becomes stationary. It can be seen that $\Pi(2|2)$ begins to decrease around $d=60$, and $\Pi(1|2)$ begins to increase and becomes dominant after $d=140$. This plot confirms that the neural network tends to use linear learning mode to extract linear features first, and starts to invoke the nonlinear learning mode only when linear features are insufficient to approach the goal of training.

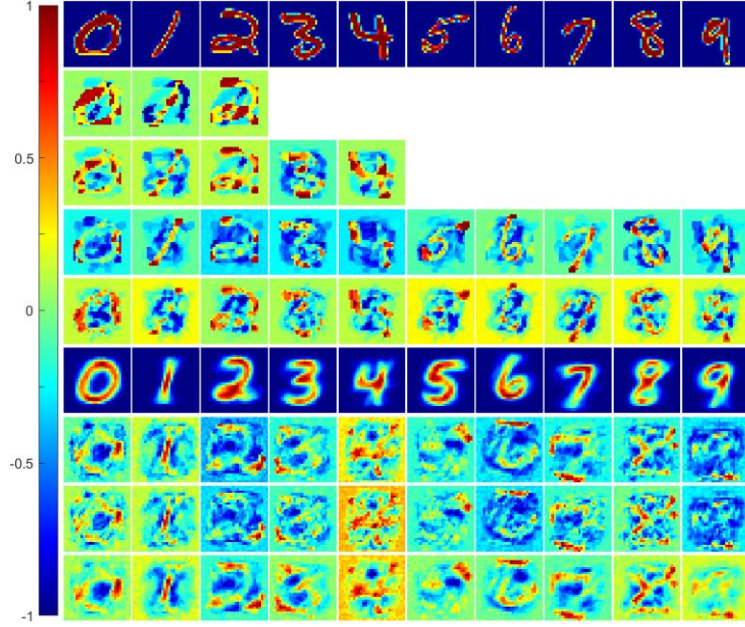


Fig. 5. The visualization of penetrating coefficients of neural networks of MINIST data set. The first line: ten digits picking up from the data set. Two to four lines: the radiographs of NNNs with $d=30$ trained by the first three, first five and all of the ten digits. Five line: the radiographs of the NNN with $d=75$ trained by the ten digits. Six to eight lines: the radiographs of the LNN and with $d=30$, the NNNs with $d=30$ and $d=70$, trained by 600 MINIST samples.

3 Application.

3.1 Extracting the linearly separable and inseparable features of handwritten digits.

The first row of Fig. 5 shows 10 handwritten digits selected from the MNIST set. Since each sample is composed of a 28x28 bitmap, we design a 784-600-P network with $P=3, 5, 10$ to classify the first 3, first 5, and all 10 samples, respectively, with control parameters $d=30$ and $\beta=0.15$. Radiographs of label neurons, i.e., $l_{\alpha\beta}^{(i_L,2)}(i_L)$ for $i_L = 1, 2, \dots, P$, are shown in the second to the fourth rows in Fig. 5, respectively. The radiographs are obtained after the neural network has been trained to have its cost function less than 0.01. It can be seen that in the case of only a few samples, radiographs are similar to those of the toy sample sets, i.e., patterns of all the digits in the training set distinctly appear in every radiograph, indicating that the “holographic” nature of the neural network remains. With the increase of the number of samples, the pattern of the digit corresponding to a label neuron can still positively recognized, while patterns of

other digits gradually become less distinguishable. By studying the progressive trend of radiographs from the cases of $P=3$ to $P=5$ and to $P=10$, one can realize that even for the case of $P=10$, the patterns of all the digits are indeed still there; they overlap with each other to form the negatively displayed region. In other words, the “holographic” structure exists always.

From the radiographs we see that the zones containing unit features of the labeled digit (the zones of a digit that do not overlap with other digits), which represent the main part of linearly separable feature of a digit, is positively highlighted, while the zones containing unit features of other non-labeled digits are negatively explored. The zones of the labeled digit that overlap with other digits are also positively displayed, but to a lesser degree than that of the unit features. Following the characteristic map, these kinds of patterns enhance the output of a sample on its label neuron, while suppress the outputs of samples of other classes on this output neuron. These patterns thus indicate how linearly separable feature is carried out by the linear learning mode.

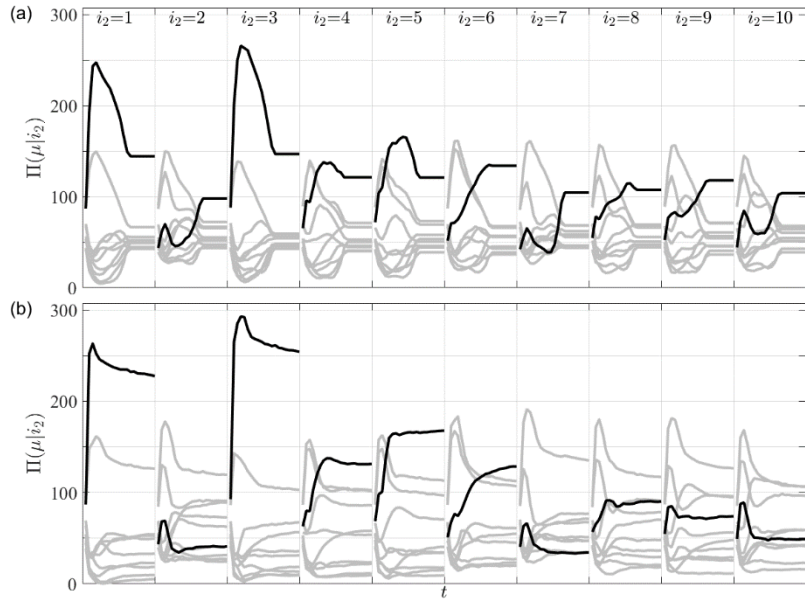


Fig. 6 The LNI for the NNNs with (a) $d=30$ and (b) $d=75$. The lines in each panel represent $\Pi(\mu|i_2)$ with $\mu = 1, \dots, 10$ for the specific output neuron i_2 ; the dark line represents $\Pi(\mu|i_2)$ with $\mu = i_2$. The time length in (a) is 8×10^6 and in (b) is 2×10^7 MC steps in each panel. .

In principle, overlapping among patterns of different classes is unavoidable, and thus there should be linearly inseparable features in every sample. Note that the zones of each digit correspond to the face zones in the toy sample sets. The fifth row of Fig. 5 shows the radiographs of the NNN obtained by learning the ten digits with $d=75$. Comparing to the case of $d=30$, we see that they are quite similar. In other words, it is difficult to verify whether the nonlinear linear mode is initiated by studying the radiographs alone. The reason is that even if there are linearly inseparable features, they will be fragmented and difficult to identify. This is different from the case of the second

sample in the third toy sample set, where the linearly inseparable feature zone is large and distinctive. However, we can still see an increasing degree of fragmentation in radiographs of $d=75$ comparing to the case of $d=30$, which may be a hint of the appearance of the nonlinear learning mode.

Solid evidences of the existence of the nonlinear learning mode can, however, be provided by the LNI. In Fig. 6, we show the evolution of the LNI of the NNN trained by the 10 handwritten digits as a function of time for $d=30$ and $d=75$. We see that in the case of $d=30$, the learning process is dominated by the linear learning mode, since the LNI satisfies the condition that $\Pi(\mu|i_2)$ is the largest for $\mu = i_2$. In the case of $d=75$, however, the LNI of five digits no longer meet this condition, indicating that the nonlinear learning mode has been initiated. This result confirms that using the cost function with a large d is an effective strategy to excite the nonlinear learning mode.

The benefit of the extraction of linearly inseparable feature can be revealed by the improvement of the accuracy of recognition. To demonstrate this effect, we train a LNN and a NNN using the first 600 samples from MNIST. Optimal parameters d and β are searched and used to generate Fig. 7(a) which shows the evolution of the accuracy rate on the supplied test set of MNIST. We can see that the test accuracy of the nonlinear network is noticeably higher than that of the linear network, although it is found that the training accuracy for both the LNN and the NNN reach 100%. These facts indicate that each training sample contains sufficient linearly separable features for successful classification, and that the training samples also contain linearly inseparable features that only the NNN is able to learn and such learnings help it to achieve a noticeable higher accuracy on the test set.

The 9th to 11th rows of Fig. 5 show radiographs of the ten output neurons for the LNN, the NNN with $d=30$, and the NNN with $d=70$, respectively. We see that patterns of digits emerge in the radiographs. The positively highlighted parts of a digit represent the zones of common linearly separable feature of a class of samples. Again, these radiographs show less distinctive feature, and we see no significant changes from the 9th row to the 11th row. As revealed by Fig. 7(a), the extra improvement of the accuracy by the NNN is about 8%. Therefore, in the case of the MNIST data set, the linear separable feature is the dominant feature, so radiographs of MNIST are dominated by linearly separable features, and thus no obvious difference can be discerned between the radiographs with or without the nonlinear learning mode.

How to maximally extract the linearly separable and inseparable features should be an essential problem for obtaining the optimal neural network. Fig. 7(b) shows the accuracy of the three-layer nonlinear network for several values of β as a function of d . Here, the accuracy at a given value of d is similar to final accuracy in Fig. 7(a), that is, with each value of d , we train the neural network to find the maximum value of the accuracy appearing in the training process. We see that, for a given β , increasing d increases the accuracy initially till it reaches the maximum value, and further increasing d actually decreases the accuracy, which is a sign of overlearning. Similarly, at a fixed d , increasing β increases the accuracy initially, but further increasing causes overlearning and the accuracy to decrease. It seems that the understanding and

controlling of overlearning is the key to the optimal solution.

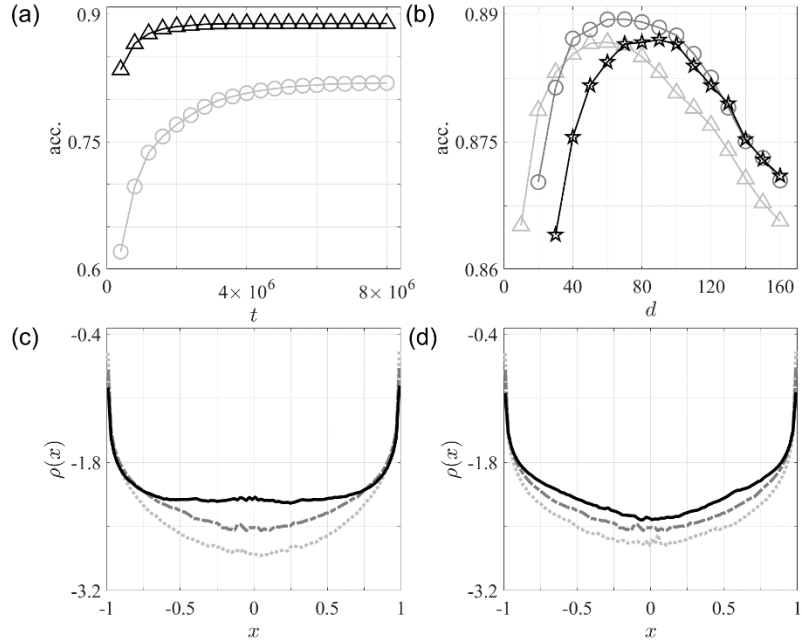


Fig. 7 Characterizing the overlearning by the distribution of outputs of hidden-layer neurons. (a) The accuracy as a function of training time for the linear (circles) and nonlinear (triangles) neural networks. (b) The maximum accuracy as a function of d for $\beta=0.05$ (triangles), 0.15 (circles) and 0.3 (stars). (c) The distribution of outputs of hidden-layer neurons for $d=40$ (solid line), 70 (dash line) and 100 (dot line) at $\beta=0.15$. (d) The distribution of outputs of hidden-layer neurons for $\beta=0.05$ (solid line), 0.15 (dash line) and 0.3 (dot line) at $d=70$.

By study of the distribution of outputs from hidden-layer neurons, we find that the overlearning induced by excessive d or β is all due to the presence of excessive number of extremely nonlinear neurons, i.e. neurons with output in the extreme nonlinearity region. In Fig.7(c) and 7(d) we show the distribution of outputs of hidden-layer neurons at $d=40,70,100$ with $\beta=0.15$, and at $\beta=0.05,0.15,0.3$ with $d=70$, respectively. In each plot, the distribution evolves from the state with less extremely nonlinear neurons to the state with more extreme nonlinear neurons. Note that the extremely nonlinear neurons are characterized by the peaks around $x=\pm 1$, and linear neurons are characterized by the distribution around $x=0$. We see that the maximum accuracy appears with a proper balance between the extremely nonlinear neurons and linear neurons. Too much or too little nonlinear neurons would both decrease the test accuracy.

Extremely nonlinear neurons are indispensable in the extracting of linearly inseparable features by the nonlinear learning mode. As shown in Fig.4, for the goal of converting the output of the second sample to have the largest value requires those of the first and third samples to cancel each other, i.e., $f(h) \approx \pm 1$ with these two samples. However, extremely nonlinear neurons do have their drawbacks; they decrease

the robustness of the neural network since they behave like the step neurons, $f(h) = sign(h)$, and too many extremely nonlinear neurons would lead to the out-of-balance between the extraction of linearly separable and inseparable features. In more detail, for a given training set, the proportion of linearly separable and inseparable features of samples is fixed. With a fixed number of hidden-layer neurons, there are two possible scenarios that may lead to a less effective neural network. One is that the total number of neurons is insufficient for extracting the complete information. Another is that the ratio of neurons with linear and nonlinear learning modes does not match that of the linearly separable and inseparable features.

With this understanding we can explain the results of Fig. 7(b). Because there is a plenty of linearly separable features, the neural network tends to invoke the linear learning mode to extract linearly separable features. If the training goal is achieved by the linearly separable features alone, the training is stopped and the test accuracy would be low because of losing the information contained in linearly inseparable features. With the increase of β , d and the training time, nonlinear neurons with extreme nonlinearity increase, leading to more nonlinear linear mode triggered and linearly inseparable feature extracted, and thus the accuracy is improved. However, excessive extremely nonlinear neurons would lead to the out-of-balance between the linear and nonlinear learning modes, and results would be overlearning.

3.2 Increasing the width or depth of neural networks to balance the linearly separable and inseparable features.

Then the remaining questions are what is the optimal distribution and what factors determine the optimal distribution. We will show that increasing the width and the depth of neural networks provides two effective ways to obtain the optimal distribution.

To show the width effect, we study a 784- N_1 -10 neural network trained by the first 600 MINIST samples with $\beta=0.15$. Here, the value of β is the optimal value from the last section with $N_1=600$, and it is checked this value remains optimal for N_1 s used in this section. In Fig 8(a), the circles and triangles show the accuracy as a function of d with $N_1=1200$ and $N_1=1800$, where each data point is the highest accuracy achieved at each value of d . Fig. 8 (b) shows the optimal accuracy as a function of the width where an optimal d is searched and used in its calculation. We see that the accuracy increases with the increase of width and gradually tends to saturation around $N_1=1500$.

In Figure 8(c), we show the distribution of outputs of hidden-layer neurons for $N_1=1200$ and 1800. Fig. 8(d) shows the height of peaks \bar{h} (averaged with the values of $x=\pm 1$) as a function of the width. It can be seen that \bar{h} decreases with N_1 .

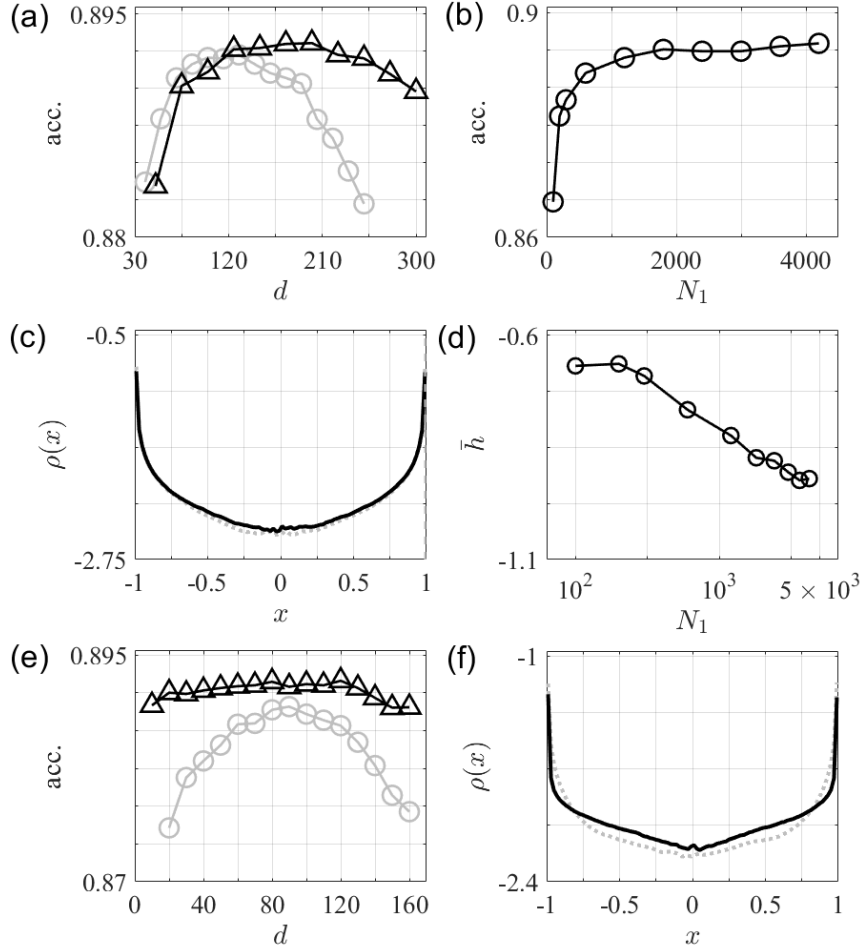


Fig. 8. The width and depth caused improvement of the network performance. (a) The accuracy as a function of d for $N_1=1200$ and $N_1=1800$. (b) The maximum accuracy as a function of N_1 . (c) The distribution of outputs of hidden-layer neurons for $N_1=1200$ and $N_1=1800$ at the maximum accuracies. (d) The height of the picks of the distribution as a function of N_1 with the log-log scale. (e) The accuracy as a function of d for the four- and five- layer neural networks. (f) The distribution of outputs of first hidden-layer neurons for the four- and five-layer neural networks.

The reason that bigger widths improve test accuracies can be understood on the basis of balancing the extraction of linearly separable and inseparable features. The amounts of linearly separable and inseparable features in the training set are fixed. With a small-size neural network, it does not have sufficient neurons to extract completely both linear and nonlinear features. As the linearly separable features are dominant, the network is inclined to use more neurons to extract this kind of information, leading to an insufficient number of nonlinear neurons and a suboptimal small ratio of extremely nonlinear neurons. With the increase of the width, there are more neurons available and thus some of them can be spared to extract the linearly inseparable features, and thus the ratio of extremely nonlinear neurons can increase to an optimal value. However, we

can expect that the total number of the nonlinear neurons used for extracting the linearly inseparable feature should stay approximately constant for even larger width; we denoted this number as N_{non} . The reason is that, as shown in Fig.4, the nonlinear learning mode requires the combination of different neurons and thus occupies more resources of the neural network. Therefore, further increasing of the width would not increase the number of neurons that extract linearly inseparable features. As a result, one can expect that the ratio of extremely nonlinear neurons, characterized by the amplitude of peaks around $x=\pm 1$ to decrease as $N_{non}/(N_1 - N_{non})$ or scale as $1/N_1$ if N_1 is large enough; the extra neurons should concentrate towards the region of $x=0$. These predictions are confirmed by Fig. 8(c) and 8(d). In these situations, neurons for extracting both linearly separable and inseparable features are approximately saturated; therefore, continuing increase of the width does not increase the test accuracy significantly as can be seen in Fig. 8(b). In summary, with a sufficient width, the neural network has the possibility to extract both linearly separable and inseparable features while keeping the balance between the linear and nonlinear learning modes.

To show the depth effect, we study a four-layer 784-600-600-10 neural network and a five-layer 784-600-600-600-10 neural network. Fig. 8 (e) shows the accuracy of these two neural networks as a function of d , and Fig. 8(f) shows the output distribution of neurons in the first hidden layer. Together with the result of the three-layer neural networks shown in Fig. 7(b), we see that the test accuracy increases with the depth of the neural network, while the number of extremely nonlinear neurons decreases with it.

Comparing Fig. 8(e) and Fig. 8(a), we see an important advantage of a deeper-layer neural network over a wider-layer one for practical applications. As shown in Fig. 8(a), the optimal value of d increases with the increasing width quite significantly. To obtain the optimal test accuracy of a wider neural network, one would have to search in a wide range for the optimal d . In contrast, as shown in Fig. 8(e), the optimal value of d does not change with the increasing depth of the neural network. In fact, there is a wide range of d that would give approximately optimal test accuracy for five-layer neural network (triangles). It is difficult for us to apply our MC algorithm to training neural networks with more layers, but from the trend exhibited by the three to five-layer neural networks, we can speculate that, with the further increase of the depth, the optimum solution region should appear as a perfect plateau over a large range of d values. As a result, it would be much easier to obtain the optimal solution by sparsely sampling the control parameter space. Furthermore, once an optimal control parameter is found, one would not have to search it again for networks with deeper depths. This property is very favorable for neural networks using the softmax cost function. We suspect that this property may be at least one of the superiorities of the deep-layer neural networks.

The mechanism that the accuracy increases and the number of extremely nonlinear neurons decreases with the increasing the depth is similar to that of increasing the width, since increasing layers also increases the total number of neurons in the network. In the last row of Fig. 5, we show the radiographs of the ten output neurons of the four-layer neural network, which indicate that the “holographic” structure of the network is remained. From the point of view of weight pathways, a deep-layer neural network has

much more weight pathways comparing to a three-layer neural network with the same number of hidden-layer neurons. For example, a 784-1200-10 network has $784 \times 1200 \times 10 \sim 9 \times 10^6$ weight pathways, while a 784-600-600-10 network has $784 \times 600 \times 600 \times 10 \sim 3 \times 10^9$ weight pathways. Therefore, deep-layer networks have much more freedom to establish subnetworks, and should provide more freedom to construct learning models. This should be the reason that a deep-layer neural network can have the nonlinear linear modes with a relatively small d . The details of this mechanism is still to be investigated in the future.

5 Degree of attention of learning process.

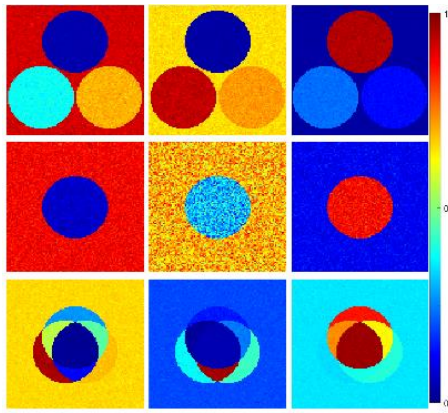


Fig.9 Visualization of the attention degree for the NNN with $d=30$. The first, second and third lines are for the first, second and third training sample sets, and the first, second and third columns are for the first, the second and the third samples.

As an augmentation to the WPA, we introduce the attention degree to monitor activities of weight mutations in this section. This concept is benefited by the MC training algorithm we adopted. The attention degree can reveal and study the contributions or weights of different features. It is defined as follows: for the mutation of weight $w_{i_1 i_0}^{(1)}$, if it maximizes the increment of local fields of all output neurons in the direction of i_L -class, then the mutation is defined as a successful attention of feature bitmap i_0 on class- i_L , and then let $P(i_0|i_L) \rightarrow P(i_0|i_L) + 1$. During or after the training, we plot the heatmap

$$l_{\alpha\beta}^{\text{att}}(i_L) = P(M\alpha + \beta|i_L),$$

to visualize the degree of attention. Fig. 9 shows the heatmaps of the degree of attention of the NNN30 for the three sample sets. The information involved in other plots can be easily interpreted.

The visualized degree of attention can explore many details of learning and learning process. Particularly, we find that there exist two modes of attention, namely,

the face attention mode and the ground attention one. In Fig 9, we see that the degree of attention for different region is different. For the first sample of the first sample set, the background has the largest degree of attention, while the face regions of the first sample has a attention that is larger than that of the third but smaller than that of the second. Therefore, to establish the subnetwork for the first sample to the first output neuron, the attention is indeed focused on the background. We call this mode the background attention mode. For the third sample, on the contrary, we see that the face zone of the third sample has the largest attention, while the other regions have less degree of attention. We call this mode the face attention mode. It can be find that the training performs the background attention for the second sample of the first set, the first and the second samples of the second set, and the first sample of the third set, while performs the face attention model for the others. Indeed, it can be realized that the degree attention has a complex structure, particularly for samples with complex features. For example, for the second sample of the third set, an extremely high degree of attention is focused on the cross area of the face zones of the first and the second samples.

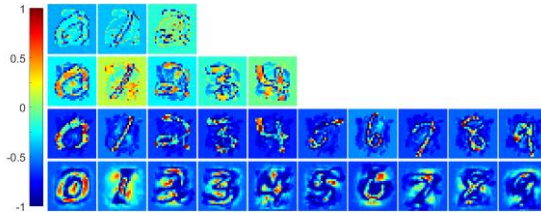


Fig. 10. The visualization of the degree of attention. First to third lines: the visualization images of the attention degree for the NNN with $d=30$ trained by the first three, the first five, and all of the ten digit samples shown in the first line of Fig. (7). The last line shows the results of the NNN trained by 600 MINIST samples.

Usually, the identifiable information lies in regions of both the target and the background. In the limit when it has $x_{i_0}(\mu) \rightarrow 0$ in the face zone, the neural network have to recognize the samples completely through the geometry of the background, while in the opposite case of $x_{i_0}(\mu) \rightarrow 0$ in the ground region, the geometry of the face becomes the only recognizable feature of the sample, and the recognition should be performed by the face attention mode. Generally, these two modes of attention are coexisted, which is similar to the way that the brain recognizes objects.

As can be seen, for example, from the heat maps of a specific sample that the value of the degree of attention of the face zone of other samples is not zero, which means that to identify a sample needs also the information of others. This proves the fact revealed by the weight-path analysis that the subnetworks of each sample stores also the information of others, i.e., holographic feature of the neural network.

The degree of attention is also helpful for analysis the learning process for the MINIST data set. In the first to third lines of Fig. 10 we show the visualized degree of attention for the first three, first five and all of the ten digit samples shown in the first

line of Fig. 7. In the last line of Fig. 10 we show the results for the first 600 samples respect to the ten output neurons. We can see that there exist also background attention mode (the second plot in the second line) and the face attention mode (all others). In addition, the unitary features of a sample, as well as those features having high degree of overlap with other samples, are usually payed more attentions.

6 SUMMARY AND DISCUSSION

Weight pathways connect inputs to outputs of a neural network through subnetworks that are characterized by penetration coefficients; any internal change of the network can be qualitatively displayed by the changes of such penetration coefficients. Therefore, the WPA approach provides an effective means to detect the internal structure of the network. In more details, with neurons as nodes, the network can be decomposed into a series of subnetworks, each of which is characterized by a characteristic map with a set of penetration coefficients. The training process can be interpreted as the organization of weight pathways to produce the minimum cost function, creating coherence structures for the penetration coefficients that represents the enhancement or suppression on the corresponding component of the input vector. With the visualization of the penetration coefficients, we gain a penetrating view of the inside of the "black box" of a neural network, making its learning and recognition mechanisms interpretable. One of the important findings through the visualizations is that each subnetwork uses a "holographic" structure to encode all the training samples instead of just one class of samples. The "holographic" structure reveals how recognition is performed, that is, when an input vector is presented, every subnetwork reacts to the whole information in it with its "holographic" structure and decides collectively what the input vector is or is not. The "holographic" structure is also the basis of the generalization capability of the neural network. Our findings support the latest neurobiological understanding of the biological neural networks in the brain [22,23], and confirms that information is stored in the networks of weight pathways.

The WPA approach reveals the self-organizing classification of the hidden-layer neurons. After the self-organization, hidden-layer neurons can be generally divided into dominant-mode neurons and auxiliary neurons. The former produce the largest output in the label neuron of an input vector, while the latter adjust the local fields of the other output neurons to approach their goal of training values. The analysis of the classification of the hidden-layer neurons leads to the finding of the linear and the nonlinear learning modes. The former extracts linearly separable features and can be performed by single neurons independently. The latter can extract linearly inseparable feature and requires the cooperation of neurons and the help of the nonlinearity of the neuron transfer function.

The WPA approach not only reveals what to learn and how to learn, but also reveals how to learn better. What to learn and how to learn? Extract the linearly separable features with linear learning mode, and extract linearly inseparable features

with nonlinear learning mode. How to learn better? Maximize the extraction of linearly separable and inseparable features and avoid the overlearning. Our study shows that a neural network tends to first extract linearly separable features with the linear learning mode. If each sample contain sufficient linearly separable features, the network may reach the training goal relying only on the linear learning mode, thus wasting linearly inseparable feature.

In order to extract linearly inseparable feature, the network needs invoke the nonlinear learning mode with a cost function that is difficult to minimize with only the linearly separable features. To maximum utilize the information of the samples, the neural network must extract both features completely and with the right balance. We demonstrate that increasing the width and depth of the network are effective strategies for this purpose. When the width of a network is large enough, there are enough neurons to support both the linear and nonlinear learning modes, and thus one has a good chance to extract both features completely. Increasing the depth of the network can also increase the probability of nonlinear learning mode, and improve the network performance. More importantly, we find that increasing the depth of a network can get the optimum performance relatively easier than increasing the width. In more details, the optimum control parameters stay approximately constant for different depths, hence the careful search for the control parameters is not necessary. This property is very beneficial for applications. We have not studied in detail neural networks with deeper layers, other types of neuron transfer function, other updating algorithms, or other types of networks. We hope such studies can be shown in future.

ACKNOWLEDGEMENTS

This work is supported by the NSFC (Grants No. 11975189, No. 11975190)

Author contributions:

H.Z. proposed the idea of WPA; F.S. performed all the simulations and proposed the idea of the degree of attention of learning; all authors contributed significantly to analysis with constructive discussions and manuscript preparation; H.Z., F.M. and F.S. wrote the manuscript.

Reference

- [1] L. Yann, Y. Bengio, G. Hinton, Deep Learning, *Nature*, 521, 436-444 (2015).
- [2] T. Poggio, A. Banburski, and Q. Liao, Theoretical issues in deep networks, *PNAS*, 117(48), 30039(2020).

[3] C. Zhang, S. Bengio, M. Hardt, B. Recht, and O. Vinyals, , Understanding deep learning (still) requires rethinking generalization. *Communications of the ACM*, 64(3), 107(2021).

[4] G. Alain, Y. Bengio. Understanding intermediate layers using linear classifier probes, arXiv:1610.01644, 2016.

[5] M. Gabrie, A. Manoel, C. Luneau, J. Barbier, N. Macris, F. Krzakala, and L. Zdeborova, *Journal of Statistical Mechanics: Theory and Experiment* 2019, 124014 (2019).

[6] R. Shwartz-Ziv, N. Tishby, Opening the black box of deep neural networks via information, arXiv:1703.00810, 2017.

[7] S. Chung, D. D. Lee, and H. Sompolinsky, *Physical Review X* 8, 031003 (2018)

[8] F. Gerace, B. Loureiro, F. Krzakala, et al. Generalisation error in learning with random features and the hidden manifold model, arXiv:2002.09339, 2020.

[9] Y. Yoshida, R. Karakida, M. Okada, and S.-I. Amari, *Journal of Physics A: Mathematical and Theoretical* 52, 184002 (2019).

[10] T. Hou and H. Huang, Statistical physics of unsupervised learning with prior knowledge in neural networks, *Physical Review Letter* 124, 248302(2020).

[11] S. Mei, A. Montanari, and P.-M. Nguyen, *PNAS* 115, E7665 (2018).

[12] D. Bau, J.-Y. Zhu, H. Strobelt, A. Lapedriza, B. Zhou, and A. Torralba, “Understanding the role of individual units in a deep neural network,” *PNAS*, 117(48), 30071 (2020).

[13] W. Samek, G. montavon, S. Lapuschkin, CJ. Anders, and K. Mueller, Explaining deep neural networks and beyond: A review of methods and applications, *PROCEEDINGS OF THE IEEE* 247 109(3), 2021.

[14] AM. Saxe, JL. McClelland, S. Ganguli, Exact solutions to the nonlinear dynamics of learning in deep linear neural networks, arXiv:1312.6120, 2013.

[15] S. Arora, N. Cohen, W. Hu, Y. Luo, Implicit regularization in deep matrix factorization, *Advances in Neural Information Processing Systems* 32, 7413(2017).

[16] C. Olah, A. Satyanarayan, I. Johnson, S. Carter, L. Schubert, K. Ye, and A. Mordvintsev, The building blocks of interpretability, *Distill* 3, no. 3 (2018): e10.

[17] D. Bau, B. Zhou, A. Khosla, A. Oliva, and A. Torralba, Network dissection: Quantifying interpretability of deep visual representations, In *Proceedings of the IEEE conference on computer vision and pattern recognition*, pp. 6541-6549 (2017).

[18] L. Phillips, G. Goh, and N. Hodas, Explanatory Masks for Neural Network Interpretability, arXiv:1911.06876,2019.

[19] D. Kalimeris, G. Kaplun, P. Nakkiran, B. Edelman, T. Yang, B. Barak, H. Zhang. "Sgd on neural networks learns functions of increasing complexity." *Advances in Neural Information Processing Systems* 32, 3496(2019).

[20] W. Hu, L. Xiao, B. Adlam, and J. Pennington, The surprising simplicity of the early-time learning dynamics of neural networks, arXiv:2006.14599, 2020.

[20] H. Zhao, A general theory for training learning machine, arXiv:1704.06885 (2017).

[21] H. Zhao, Inferring the dynamics of “black-box” systems using a learning machine, *Science China Physics, Mechanics & Astronomy* 64, 270511(2021).

[22] L. F. Barrett, *Seven and a half lessons about the brain*, Houghton Mifflin Harcourt

Publishing, NY, 2020

[23] J. Cepelewicz, The Brain Doesn't Think the Way You Think It Does, Quanta Magazine, 24 Aug 2021 (<https://www.quantamagazine.org/mental-phenomena-dont-map-into-the-brain-as-expected-20210824/>)